Macromolecules

pubs.acs.org/Macromolecules Article

Magneto-Responsive Nanocomposites with a Metal−Ligand Supramolecular Matrix

Liuyin Jiang,[‖] Pablo Griffiths, Julie Balouet,[‖] Titouan Faure, Rowanne Lyons, Charles-André Fustin,* and Guilhem P. Baeza*

Cite This: https://doi.org/10.1021/acs.macromol.2c00256 Read Online

ACCESS | Metrics & More | Article Recommendations | Supporting Information

ABSTRACT: Magneto-responsive nanocomposites are prepared by mixing 1−5 vol % of Fe nanoparticles (NPs) in a metallo-supramolecular network made of poly(*n*-butyl acrylate) (PnBA) bearing terpyridine side groups and cross-linked by the addition of different amounts of Zn^{2+} ions. To have a clear understanding of the stepwise increase of complexity, the thermomechanical behavior of these materials was characterized through shear linear rheology at each step of their preparation. The metallo-supramolecular networks reveal a clear transition from polymer- to network-driven dynamics when passing progressively from low (<0 °C) to high temperature. While terpyridine (TPy)−Zn^{2+} complexes are usually treated as independent "stickers", the analysis of our master curves strongly suggests their aggregation. After the addition of 1−5 vol % of Fe nanoparticles within the supramolecular networks, we evidence the presence of TPy−NP bonds, resulting in a hybrid network of much longer relaxation time. Lastly, we combine thermal imaging and induction heating to emphasize the signature of sticker dissociation, offering new technical solutions to deepen our fundamental understanding of supramolecular networks.

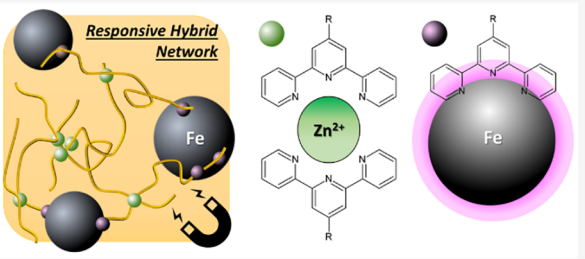

1. INTRODUCTION

Since the attribution of the Nobel Prize in Chemistry to Cram, Lehn, and Pedersen for their pioneering research on supramolecular chemistry, the interest of the scientific community for supramolecular materials has continuously grown. In particular, supramolecular polymers and networks based on various interactions such as hydrogen bonds, $\pi-\pi$ interactions, ionic aggregation, and metal−ligand complexation have since seen incredible development, notably as bases for self-healing-oriented applications.[1−5] Among these supramolecular interactions, metal−ligand interactions are particularly interesting because their characteristics (binding strength, lifetime) can be tuned over several orders of magnitude simply by changing the metal ions and/or the ligand.[6,7] Among a myriad of available ligands, terpyridine (TPy) has been widely used to form a variety of supramolecular polymers and networks because of its relatively easy synthesis, existence of several commercially available derivatives, and ability to coordinate with a broad range of transition metal ions.[8−15]

The introduction of supramolecular interactions into polymer materials is thus a popular strategy to tune their mechanical properties or confer them with desirable properties such as self-healing or recyclability. However, it also introduces some drawbacks such as a greater sensitivity to external perturbations (e.g., moisture[16]) or to creep. To overcome these limitations, the concepts of dual and double networks have been proposed.[17,18] While different in design principle, they share a common concept, the combination of at least two distinct dynamic modes within the same material aiming to display multiscale viscoelastic responses under the influence of an external stress or deformation field. Consequently, they are characterized by a "double" mechanical behavior, which offers a better balance between the desired properties. Dual networks are usually built from one polymer cross-linked by two types of interactions, either two different types of supramolecular interactions (or dynamic covalent bonds) or a combination of supramolecular and covalent cross-links.[19−23] Double networks, on the other hand, are a special subclass of interpenetrated networks where the two subnetworks show large differences of cross-linking density. The first highly cross-linked sacrificial network provides toughness to the material, while the second loosely cross-linked network provides it with shape persistence and extensibility.[24−26] The original examples were built using only covalent cross-linkers, but later examples of fully supramolecular double networks, or hybrid covalent-supramolecular systems, were reported.

Received: February 4, 2022
Revised: April 19, 2022

https://doi.org/10.1021/acs.macromol.2c00256
Macromolecules XXXX, XXX, XXX−XXX

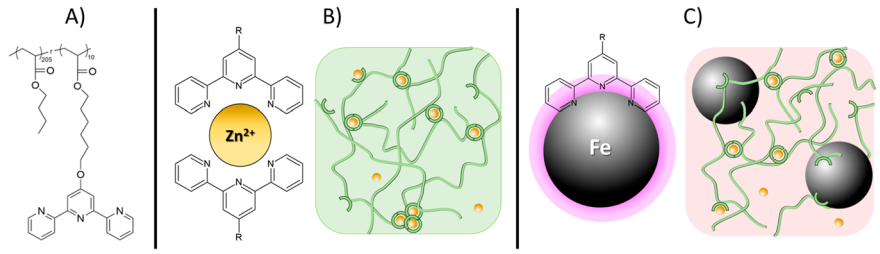

Figure 1. (A) Molecular structure of the PnBA−TPy random copolymer used in this work. (B) Schematic representation of the metal−ligand interaction between Zn^{2+} and the terpyridine ligands and the corresponding network structure. (C) Schematic representation of the interaction between a terpyridine ligand and an Fe NP and the corresponding network structure. The purple halo represents the corresponding composites.

Table 1. Details on the Samples' Formulations

name	TPy/chain	T_g[a] °C	$\overline{M_n}$ (GPC) kg mol^{-1}	$Đ$ (GPC)	[Zn]/[TPy]	Φ[b] (vol %)
PnBA	0	−48.5	25	1.1	0	0
PnBA−TPy	10	−38.1	30	1.2	0	0
PnBA−TPy(0.25)		−37.4			0.25	0
PnBA−TPy(0.35)		−37.8			0.35	0
PnBA−TPy(0.5)		−37.5			0.5	0
PnBA−TPy(1.35)		−38.8			1.35	0
PnBA−TPy(2)		−38.5			2	0
PnBA−TPy(0.5)-1%		−38.0			0.5	1
PnBA−TPy(0.5)-3%		−37.6			0.5	3
PnBA−TPy(0.5)-5%		−37.7			0.5	5
PnBA−TPy(2)-1%		−38.6			2	1
PnBA−TPy(2)-3%		−37.8			2	3
PnBA−TPy(2)-5%		−36.8			2	5

[a]Glass transition temperature, extracted from eq 1 applied to the DSC data (see Figures 4 and 7). Neat PnBA data are not shown. [b]Volume fraction of Fe NPs.

This multidynamic concept is further used for the design of tough hydrogels particularly useful in bioengineering, including in the case where silica nanoparticles (NPs) play the role of multifunctional cross-linking points.[27,28] Besides, the addition of NPs as physical cross-links is quite common in material science to prepare "attractive nanocomposites", where the high interfacial surface between the polymer matrix and the fillers ensures a strong effect on the properties with a limited NP content. A popular and thoroughly studied example is that of poly(2-vinylpyridine) reinforced with silica NPs in which multiple hydrogen bonds dramatically slow down the dynamics of the polymer from the segmental[29,30] up to the terminal relaxation[31] and increase the plateau modulus exponentially with the filler content.[31,32] Other examples based on poly(propylene glycol), poly(vinyl acetate), and glycerol can be found in the work of Cheng and Sokolov.[33] Beyond, even more advanced versions of attractive nanocomposites have been proposed. For example, iron or iron oxide NPs were used to thermally trigger the desorption of polymer chains (resulting in corresponding macroscopic flow) upon the application of an external oscillatory magnetic field.[11,34] Although all these "NP-crosslinked" materials are not necessarily expected to be endowed with rapid self-healing (i.e., spontaneous-healing) ability because of their long terminal relaxation time, their enhanced properties combined with possible stimulus-induced healing open perspectives for the development of many applications in the future.

With these ideas in mind, we develop in the present work responsive hybrid supramolecular networks that may serve as stimulus-healable rubbers. Similarly as in dual networks, the idea consists of generating two kinds of supramolecular interactions within the material. Here, TPy-functionalized poly(*n*-butyl acrylate) (PnBA) serves as the polymer matrix, capable of forming supramolecular complexes with Zn^{2+} and Fe NPs. The unentangled nature of the polymer directs more focus toward the role of each type of bond instead of the intrinsic property of the polymer and ensures a rapid solid-to-liquid transition upon induction heating, which is useful for healing purposes. From a more fundamental point of view, particular attention is paid to the corresponding gigantic drop of viscosity that makes NPs free to move and dissipate extra-heat through mechanical friction. In fact, by following the temperature evolution during induction heating, it seems possible to detect supramolecular group dissociation through thermal imaging.

The Article is organized as follows. After the Materials and Methods section, we present the rich thermomechanical behavior of unfilled polymer networks where the effect of the Zn^{2+} concentration is characterized in depth through rheology and calorimetry. The operation is then repeated on hybrid networks consisting of both TPy−Zn^{2+} and TPy−Fe NP interactions. Lastly, induction heating experiments are discussed as an original tool enabling one to probe sticker dissociation.

2. MATERIALS AND METHODS

2.1. Materials. $ZnCl_2$ (reagent grade) was purchased from Sigma-Aldrich (USA). Acetone (analytical grade) and methanol (analytical grade) were purchased from Carlo Erba (Italy). The magnetic iron powder made of polydisperse NPs (average diameter of 90 nm) was purchased from Nanografi (Turkey) and directly used without further surface treatment.

https://doi.org/10.1021/acs.macromol.2c00256
Macromolecules XXXX, XXX, XXX−XXX

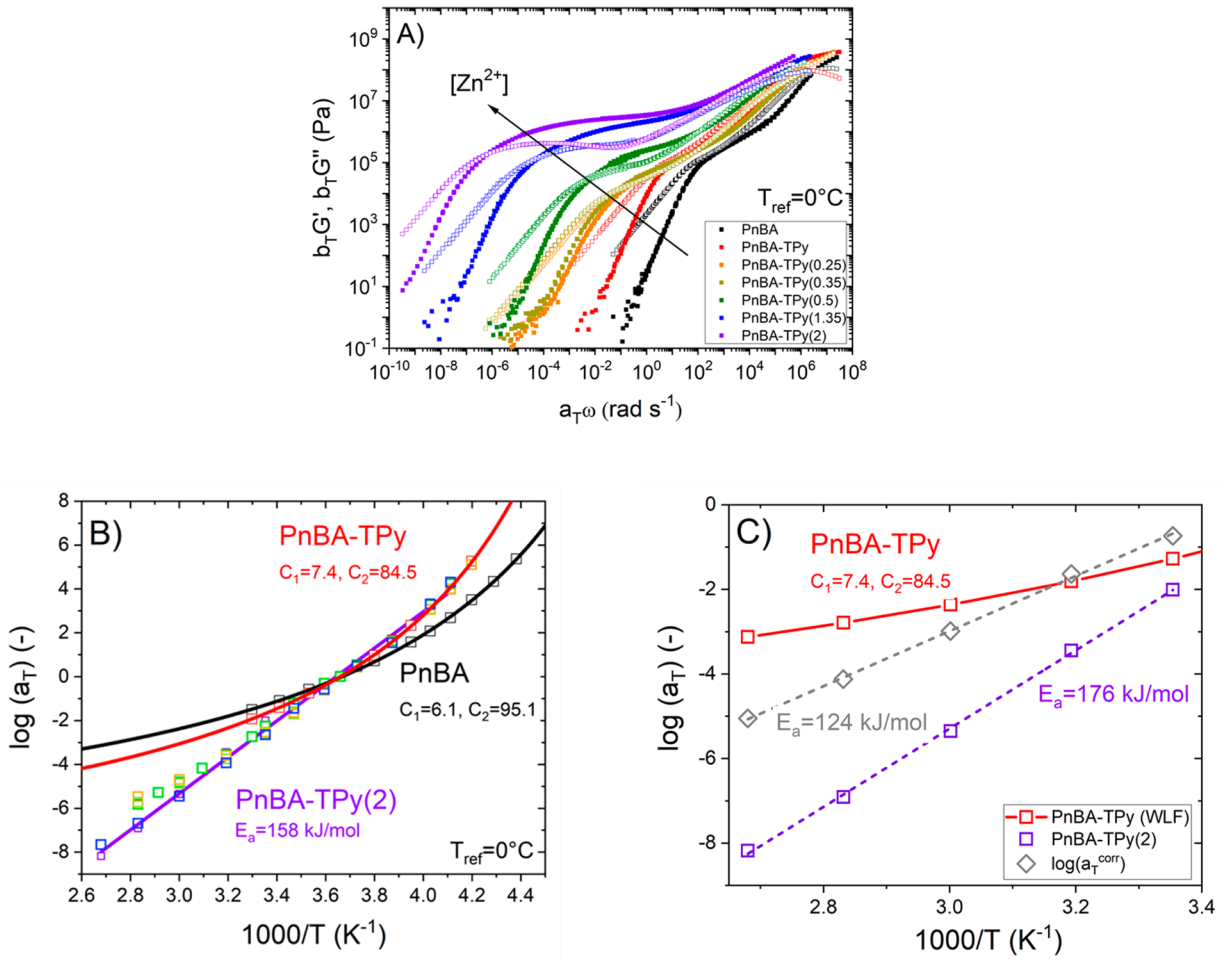

Figure 2. (A) Rheology master curves on a series of metallo-supramolecular networks and corresponding neat polymers. The reference temperature is 0 °C. (B) Corresponding temperature dependence of the horizontal shift factor a_T. Black, red, and purple solid lines are WLF fits on PnBA and PnBA−TPy and an Arrhenius fit of PnBA−TPy(2) data, respectively. Fit parameters are displayed in each case; c1 and c2 values of PnBA and PnBA−TPy are significantly different due to the high density of TPy side groups in the latter (1 group/3 kg mol^{-1}). (C) Analog data and corresponding corrected shift factor (see text).

2.2. Polymer Synthesis. Random copolymerization of n-BA and terpyridine functionalized monomer was performed by reversible addition−fragmentation chain transfer polymerization (RAFT) under bulk conditions at 70 °C using 2-(dodecylthiocarbonothioylthio)-2-methylpropionic acid (DDMAT) as RAFT agent following a previously reported procedure.[11] Briefly, AIBN (3 mg, 18.3 μmol), DDMAT (44.5 mg, 0.122 mmol), n-BA (3.37 mL, 23.8 mmol), and acrylate-TPy (535 mg, 1.44 mmol) were introduced into a 10 mL Schlenk tube. After the solution was degassed by six freeze−pump−thaw cycles, the reaction mixture was sealed, purged with argon, and then immersed in a preheated oil bath at 70 °C. The polymerization was stopped at a monomer conversion of 82% by immediate exposure to air and cooling with liquid nitrogen. The copolymer was purified by precipitation in a methanol/water (85/15) mixture. The final composition was determined to be PnBA205−r-Tpy10 (Figure 1A) from GPC (using PS standards) and ^{1}H NMR analyses (the numbers are the average number of repeating units). The PnBA homopolymer was synthesized in a similar way. Molecular characteristics of the polymers are provided in Table 1.

2.3. Supramolecular Network Preparation. A desired quantity of polymer was first dissolved in a minimum amount of acetone (400−500 mg/mL). In a separate vial, a stock solution was prepared by dissolving $ZnCl_2$ in methanol. Depending on the targeted molar ratio between Zn^{2+} and TPy, a given amount of the $ZnCl_2$ stock solution was added to the polymer solution and mixed by vortex for 5 min. Solvents were subsequently removed by rotary evaporation and further dried under vacuum at 40 °C overnight.

2.4. Nanocomposite Preparation. Nanocomposites of PnBA−TPy, $ZnCl_2$, and Fe NPs were made by first preparing a PnBA−TPy and $ZnCl_2$ solution mixture as described in the previous section. On the basis of the volume fraction of the nanocomposite, a desired amount of Fe NPs was weighed into a vial and suspended using acetone followed by sonication for 10 min. The prepared Fe NP suspension was subsequently transferred into the PnBA−TPy and $ZnCl_2$ solution mixture and sonicated for a further 10 min. The solvent was quickly removed by rotary evaporation to enhance the viscosity and limit the dramatic sedimentation of the NPs. The resulting nanocomposite was further dried under vacuum at 40 °C overnight.

2.5. Rheology. Dynamic frequency sweeps (100−0.1 rad s^{-1}) were performed on neat polymers and supramolecular networks every 5 or 10 °C from 100 °C down to −30 °C with an ARES G1 (TA, USA) equipped with 8 mm diameter stainless steel parallel plates under air. At low temperatures, compliance issues were corrected on the basis of the work of Laukkanen[35] in a similar way as in our previous paper.[11] Master curves were built on the whole temperature range by following the time−temperature superposition principle. First, $G'(\omega, T)$ and $G''(\omega, T)$ data were shifted horizontally so that the corresponding tan $\delta(T) = G''(\omega, T)/G'(\omega, T)$ data matched its counterpart measured at the reference temperature tan $\delta(T_{ref})$. Second, the horizontally shifted $G'(\omega, T)$ and $G''(\omega, T)$ were shifted

https://doi.org/10.1021/acs.macromol.2c00256
Macromolecules XXXX, XXX, XXX−XXX

vertically so that they matched, respectively, nonshifted $G'(\omega, T_{ref})$ and $G''(\omega, T_{ref})$. While vertical shifts never exceeded a factor of 3.3 from the lowest (−30 °C) to the highest temperature (100 °C), the entropy elasticity theory [$b_T = (\rho_{ref}(T_{ref})T_{ref})/(\rho(T)T)$] rather provides a factor of 1.4 in the same conditions. We believe that this discrepancy is strongly related to the thermorheological complexity of our (dense) supramolecular networks that significantly impact the time−temperature superposition procedure when passing from high temperature to the Rouse relaxation regime and below (see SI Section 1). In fact, a restriction of the shifting procedure to the low temperature range (−30 to 25 °C) matches the theory well.

In the present study, we arbitrarily set the reference temperature to 0 °C, corresponding to the Rouse relaxation regime of neat PnBA−TPy in the usual frequency range (0.1−100 rad s^{-1}) accessible with commercial rheometers. In spite of slight discrepancies in the intermediate frequency range (around T_{ref}) caused by thermorheological complexity, the master curves we obtained following this procedure were extremely smooth. In addition, dynamic frequency sweeps (100−0.1 rad s^{-1}) were performed on nanocomposites loaded with 1, 3, and 5 vol % of Fe nanoparticles and satisfying a ratio of [Zn]/[TPy] of either 0.5 or 2 with a MCR301 (Anton Paar, AUS) at 90 °C. The strain amplitude was systematically adjusted on both rheometers to stay in the linear regime (covering a range from 0.5% to 30% according to the temperature and material's nature).

2.6. DSC. DSC measurements were carried out on a TA Instruments Q10 apparatus under 50 mL min^{-1} nitrogen flow. Temperature and enthalpy calibrations were performed using indium and zinc standards. Samples of about 10 mg were cooled down to −70 °C for 5 min before being heated up at 5 °C min^{-1} up to room temperature. This cycle was then repeated once, resulting in the measurements presented in Figure 3 (2nd heating ramp).

2.7. Induction Heating and Thermal Imaging. Induction heating of nanocomposites was performed with a master controller V3+ apparatus (CEIA, Italy) connected to a pancake-shaped (flat spiral) inductor made of two concentric turns. A 0.1 mm thick Teflon composite tape covered the inductor to protect it from material flow. The frequency of the magnetic field applied was fixed to 855 kHz and its amplitude, to ca. 6 mT, corresponding to an intensity of 19 A in the inductor. The magnetic solicitation consisted of pulses representing 17% of the experimental time, ensuring a comparison of data from all the composites while avoiding any risk of sample degradation at the highest particle content (5 vol %). Disk-shaped samples (3 mm diameter and ca. 0.3 mm thick) were heated and their temperature variations, recorded contemporaneously with a PI 450 infrared camera (Optris, Germany) equipped with a 13° lens characterized with an optical resolution of 382 × 288 pixels and a measurement rate of 27 Hz. A schematic representation of the whole disposition is presented in ref 34.

3. RESULTS AND DISCUSSION

This section is subdivided into three parts dealing, respectively, with (1) the thermomechanical behavior of neat polymers (PnBA and PnBA−TPy) and their evolution upon adding Zn^{2+} ions to form supramolecular networks, (2) the thermomechanical behavior of the supramolecular networks PnBA−TPy(2) and PnBA−TPy(0.5) loaded with 1 to 5 vol % in Fe NPs, and (3) the induction heating and thermal imaging of these two series of nanocomposites. This sequence will allow us to understand the evolving complexity of the materials, passing from neat polymers to supramolecular networks to nanocomposites in which both TPy−Zn^{2+} and TPy−NP interactions play a major role (see Figure 1).

3.1. Neat Polymers and Supramolecular Networks. In Figure 2a, we have gathered (compliance-corrected) rheological master curves of the whole set of supramolecular networks based on PnBA−TPy satisfying the [Zn]/[TPy] ratio of 0−2 as well as the corresponding data for neat PnBA and PnBA−TPy. As one may have expected from similar studies investigating the rheology of linear and star-shaped telechelic PnBA−TPy interacting through metal−ligand interactions,[10] the terminal relaxation time as well as the plateau modulus of our materials appear to increase monotonically (with no saturation) upon increasing the [Zn]/[TPy] ratio, even above the stoichiometric ratio of 0.5. This effect has been well documented and assigned to the increasing density of supramolecular bonds in the system and possibly to a partial aggregation of the charged TPy−Zn^{2+} complexes. The latter will be discussed in more detail later (see below). While neat polymers are unentangled and relax following the usual Rouse model ($G' \sim \omega^{0.5}$ and $G'' \sim \omega^{0.5}$) above their glass transition temperature, an elastic plateau progressively emerges with increasing [Zn]/[TPy], reminiscent of the presence of persistent, yet dynamic, cross-links. Besides, all the materials exhibit the usual storage and loss moduli power law dependence in the flow regime, i.e., $G' \sim \omega^2$ and $G'' \sim \omega$, strongly suggesting the negligible probability of finding active stickers or microphase separated domains at long times and high-enough temperatures (ca. 70 °C for PnBA−TPy(2)).

More anecdotally, the presence of TPy side groups along the PnBA backbone is unambiguously seen to slow down its segmental relaxation, similarly as in ref 11. This observation is supported by Figure 2b where the shift factor of PnBA−TPy diverges at lower values of the reciprocal temperature. Figure 2b further indicates that the material dynamics is dominated by the segmental relaxation of the polymer at low temperature, whereas it is clearly driven by the supramolecular bonds at higher temperatures. In fact, while the usual William−Landel−Ferry (WLF) equation well describes the evolution of the shift factor for neat polymers in the whole temperature range and for supramolecular networks below 293 K, an Arrhenius behavior is clearly observed for the networks above this threshold. Interestingly, the corresponding apparent activation energy increases slightly when increasing the [Zn]/[TPy] ratio, corroborating the aforementioned absence of saturation. More quantitatively, it is worth noting that the largest value of the apparent activation energy (158 kJ mol^{-1}) corresponds to roughly twice the bond energy of the TPy−Zn^{2+} complex as reported by Zhuge et al.[36] (81 kJ mol^{-1}). For the sake of completeness, we also display in Figure 2C the PnBA−TPy(2) shift factor in the absence of the PnBA−TPy WLF contribution, possibly corresponding to the sole contribution of the sticker dynamics. This operation can be formalized as $\log(a_T^{corr}) = \log (a_T)_{PnBA-TPy} - \log (a_T)_{PnBA-TPy(2)}$, resulting in a "corrected" activation energy of 124 kJ mol^{-1}. Although this value is still significantly higher than the one reported by Zhuge et al.,[36] it is not necessarily surprising given the high density of the TPy sticker in the present study, likely to form sticker aggregates and perturb the PnBA down to the Rouse's blob length scale. An alternative representation of this result is provided in Supporting Information (SI) Section 1, where the PnBA−TPy(2) master curve was generated using the shift factor of the neat PnBA−TPy sample. The large mismatch on both sides of the reference temperatures clearly emphasize the impact of the stickers on the polymer dynamics over ca. 10 decades of frequency.

Although building such "hybrid" master curves through the use of the time temperature superposition principle is not new (see, e.g., Cui et al.[37] and Chen et al.[38] where UPy moieties and ionomers are, respectively, studied) nor strictly correct from a theoretical point of view because of the simultaneous

https://doi.org/10.1021/acs.macromol.2c00256
Macromolecules XXXX, XXX, XXX−XXX

presence of segmental motions and sticker association resulting in "thermorheological complexity", we believe that it clearly illustrates the heterogeneous dynamics that is the main characteristic and interest of these materials. We provide all the raw data corresponding to Figure 2A in SI Section 1.

While the qualitative growth of the plateau modulus and of the terminal relaxation time are expected from the sticky-Rouse and sticky-reptation formalisms,[39] their quantitative analysis deserves closer inspection. In fact, for unentangled polymers, the presence of cross-links is expected to enhance the plateau modulus linearly, following $G_N = \rho RT/M_S$ (affine model) where M_S is the average molar mass of the polymer strands located between two supramolecular bonds (also referred to as the active sticker), ρ is the density, R is the perfect gas constant, and T is the temperature. (Note that this formalism does not account for possible entanglements between chain assemblies; since it is impossible to quantify here given the fact that a chain carries a sticker every 3 kg mol^{-1}, likely to considerably perturb its Gaussian conformation and the local polymer density.) In Figure 3A, we present the evolution of M_S, i.e., the molar mass between active stickers, as a function of [Zn]/[TPy]. This value is determined from the affine model in which G_N is taken at the frequency of the local minimum of G''/G' (see SI Section 1). Interestingly, while M_S is expectedly seen to decrease with [Zn]/[TPy] because of the densification of the network, it passes below the critical value of $\overline{M_n}/10 \approx 3$ kg mol^{-1}, corresponding to the average molar mass between TPy groups in the polymer chain as defined by the chemical structure (Table 1). These results unambiguously suggest that the affine model fails to predict the mechanical behavior of the dense networks or, in other words, that another mechanism, providing extra elasticity, should be considered.

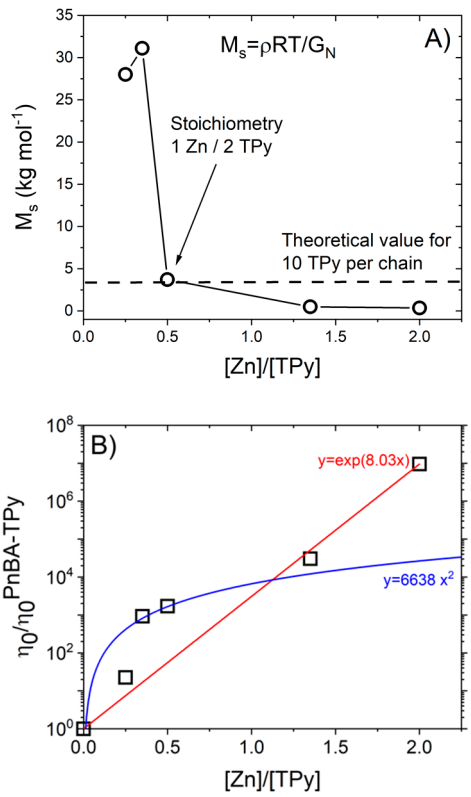

Figure 3. (A) Theoretical molecular weight between two active stickers assuming that the rubbery plateau modulus can be extracted from the affine model and that Zn−TPy bis-complexes are isolated from each other. (B) Evolution of the relative zero-shear viscosity of the supramolecular network with an increase in the [Zn]/[TPy] ratio. Solid lines are fit to the data; corresponding expressions are reported where x and y are, respectively, the relative viscosity and the [Zn]/[TPy] ratio. The X2 dependence function is expected from the sticky reptation model while we observe an exponential trend when considering the whole range of data.

In addition, the evolution of the zero-shear viscosity η_0 at T = 0 °C as a function of [Zn]/[TPy] exhibits an exponential trend (Figure 3B). However, the general scaling law of the sticky-Rouse (and sticky-reptation) models indicates that the final relaxation time should scale as the square of the number of stickers per chain (denoted S in ref 39). Interestingly, a restriction of the data fit to the first 4 points makes this scenario quite plausible, suggesting here again that another mechanism should be considered at high [Zn]/[TPy] values. The two above-mentioned unusual trends can nevertheless be rationalized by invoking the aggregation of TPy−Zn^{2+} complexes in the PnBA matrix, as already evidenced by several other studies.[8,40−42] In fact, the aggregation of stickers has two effects: (1) an increase of the functionality of supramolecular cross-linking nodes, similarly as in multiblock copolymer-based thermoplastic elastomers,[43] which provides therefore additional reinforcement, and (2) an increase of the apparent lifetime of the supramolecular bond since the relaxation of the chains will only be possible once all the TPy from an aggregate are detached. Note finally that the presence of a growing aggregation of the metal−ligand complexes with increasing [Zn]/[TPy] is in quite good agreement with the absence of saturation in terms of rheological behavior.

At a local length scale, DSC thermograms (Figure 4A) further enable the detection of important changes in the dynamics of our materials. In fact, an increase in the [Zn]/[TPy] ratio is unambiguously seen to lower the heat capacity step ΔC_p^* occurring at the PnBA−TPy glass transition. While in the neat PnBA−TPy polymer, this transition is accompanied by a massive increase of the chain segment mobility, the latter is significantly reduced in the presence of supramolecular bonds, persisting at a much longer time scale than the segmental relaxation. The effect of supramolecular bonds can also be described as a broadening of the glass transition as already described in supramolecular networks and nanocomposites probed via both DSC and dielectric spectroscopy.[29,31] This broadening is also clearly visible in the master curves (Figure 2A) in the vicinity of the segmental relaxation ($a_T\omega \approx 10^5$ rad s^{-1}). For the sake of clarity, we represent in Figure 4B the evolution of both ΔC_p^* and the transition breadth p for the various sample compositions that we extracted from fitting the DSC data with an empirical dose−response

$$C_p = C_p^0 + \frac{\Delta C_p^*}{1 + 10^{(T_g - T)p}} \quad (1)$$

where C_p^0 is the heat capacity at a temperature far below T_g. Interestingly, using this fitting method, which assigns T_g to the step inflection point, does not indicate any significant change in T_g with increasing [Zn]/[TPy], varying erratically between −38.8 and −37.4 °C (see Table 1).

3.2. "Dual" Supramolecular Network-Based Nanocomposites. In this section, we investigate the possibility of creating dual supramolecular networks based on both TPy−

https://doi.org/10.1021/acs.macromol.2c00256
Macromolecules XXXX, XXX, XXX−XXX

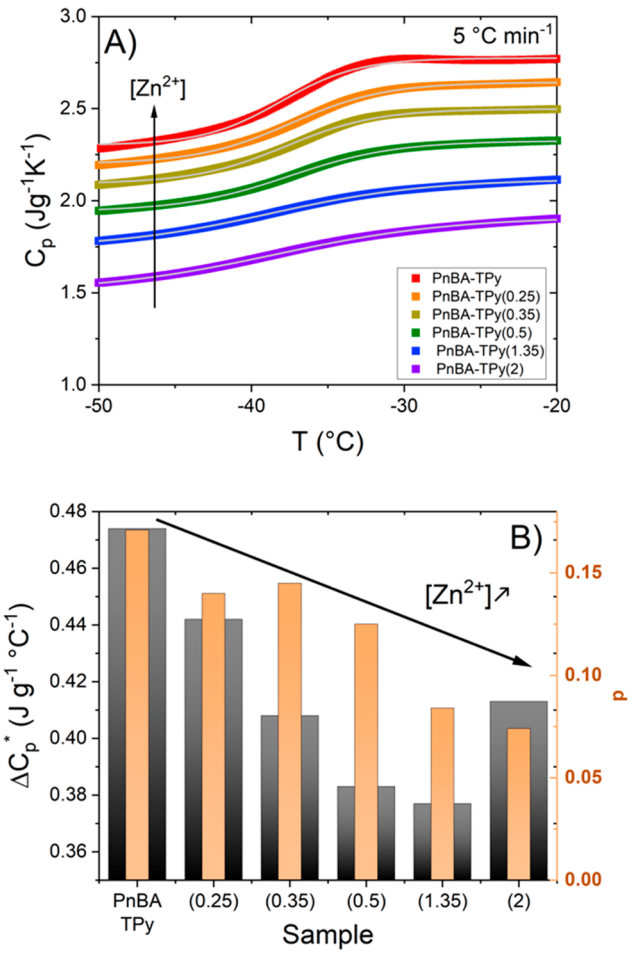

Figure 4. (A) Specific heat capacity as a function of the temperature for neat PnBA−TPy and all the corresponding supramolecular networks. Apart from PnBA−TPy, data were shifted vertically for clarity. Gray solid lines are fit to the data with the dose−response function. (B) Specific heat capacity step amplitude and slope extracted from the dose−response fit for the different samples.

Zn^{2+} and TPy−NP interactions. These responsive nanocomposites will allow us to use induction heating in view of the possible material's healing. In Section 3.3, we will then combine induction heating and thermal imaging to detect supramolecular bond dissociation.

The processing route allowing the production of PnBA−TPy nanocomposites loaded with Φ = 1, 3, and 5 vol % in Fe NPs is presented in Figure 5A (details are provided in Section 2). Interestingly, mixing the solution of PnBA−TPy and $ZnCl_2$ with a suspension of NPs in acetone results in a purple solution after a few seconds of sonication, similarly as to what is observed when mixing TPy and Fe^{2+} ions.[44] Although the exact nature of the chemical interaction is not known in this case, this observation suggests therefore that the TPy-functionalized polymer is able to interact favorably with the surface of the NPs in a similar way as with metal ions. Note that the supernatant in Figure 5A exhibits a pale pink color, probably coming from a low concentration of the smallest NPs (ca. 20 nm in diameter),[34] well-stabilized by their interactions with the polymer.

To verify this hypothesis and exclude any possibility of Fe^{2+} ion leaching from the NPs during processing, we performed additional preparation tests presented in Figure 5B. In this case, after sonicating the NP suspension, we centrifuged it to isolate the NPs from the supernatant. Then, the addition of the PnBA−TPy solution into the supernatant does not lead to any coloration, evidencing the absence of Fe^{2+} ions in the solvent and strongly supporting that the purple color of our composites does originate from TPy−NP interactions as illustrated in Figure 1C.

Because the PnBA−TPy polymer is highly sensitive to electron beams, it was difficult to obtain a clear description of the NP structure through scanning electron microscopy. Other attempts were performed on a similar material loaded with Fe_3O_4 NPs, but there again, the micrograph quality did not really allow us to properly characterize the particle dispersion.[11] In addition, the use of SAXS does not provide much information here because of the high polydispersity of the Fe NPs we used; we refer the interested reader to our previous work where these measurements are provided as Supporting Information.[34] In the same article, identical Fe NPs were used to reinforce a TPU matrix (observable with SEM and TEM) and some degree of aggregation was observed. A better dispersion is expected in the present work because of the attractive interactions between NPs and the TPy moieties of the polymer.

In Figure 6, we present dynamic frequency sweep measurements emphasizing the impact of NPs on the rheological response of PnBA−TPy(0.5) and PnBA(2) samples at 90 °C. At this temperature, while neat PnBA−TPy(0.5) exhibits a

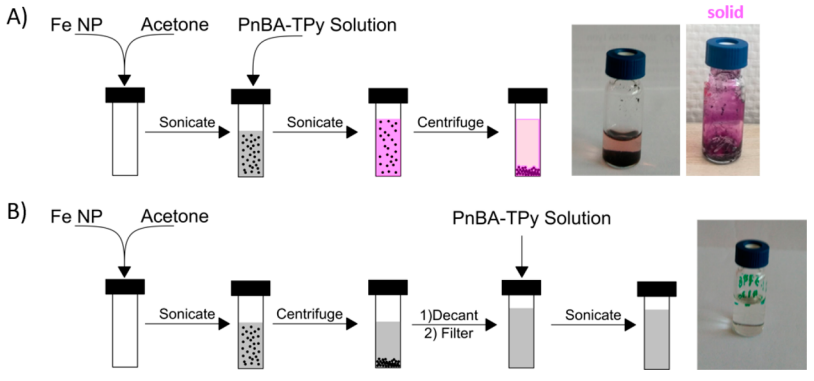

Figure 5. (A) Addition of PnBA−TPy to a suspension of Fe NPs induces a purple color. Subsequent drying makes the change in color even more obvious. (B) Analogous procedure on the sole supernatant of the same sonicated NP suspension gives no color, proving that the purple color in (A) is due to the interaction between TPy and the NPs and not to Fe ions that would have leached out of the solution.

https://doi.org/10.1021/acs.macromol.2c00256
Macromolecules XXXX, XXX, XXX−XXX

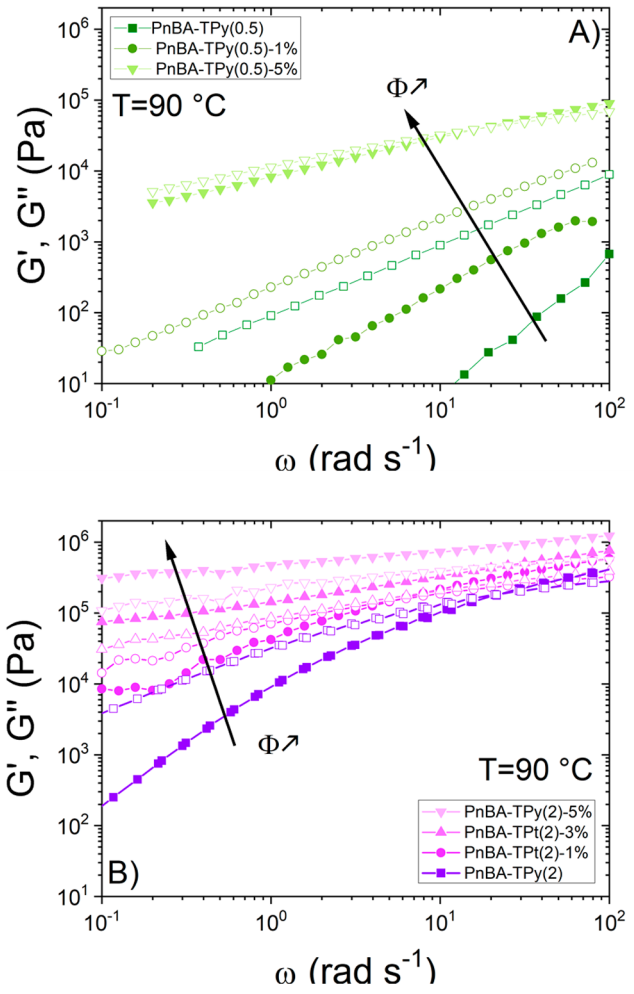

Figure 6. Storage (G', filled symbols) and loss (G'', hollow symbols) moduli as a function of the frequency of solicitation measured at 90 °C for nanocomposites and their corresponding neat matrix. (A) PnBA−TPy(0.5) and (B) PnBA−TPy(2). Note that PnBA−TPy(0.5)-3% is not reported because of a lack of material to perform the rheological experiment. PnBA−TPy(2) data is based on the master curve setting T_{ref} = 90 °C.

liquid-like response ($G' < G''$) between 0.1 and 100 rad s^{-1}, the addition of NPs progressively increases its degree of elasticity until reaching $G' \approx G''$ at 5 vol %, further supporting the presence of favorable interactions between the polymer and the NPs. More quantitatively, the increment of viscosity observed in both series of nanocomposites is far above hydrodynamics expectations $\left(\frac{\eta}{\eta_0} \gg 1 + 2.5\Phi\right)$,[45] definitely corroborating favorable polymer−NP interactions. Besides, neat PnBA−TPy(2) exhibits a much more elastic behavior than PnBA−TPy(0.5) due to its higher density of supramolecular bonds. In this case, the addition of NPs provides a significant, albeit limited, reinforcement to the material at high frequency (plateau modulus). In this regime, the polymer has not yet reached its terminal relaxation, implying that the NPs are immobilized within the network. The reinforcement can then theoretically be explained by the hydrodynamic model of Smallwood,[46] $\frac{G}{G_0} \approx 1 + 2.5\Phi$, in analogy to the above-mentioned Einstein model. Interestingly, this modest, but "positive", reinforcement further suggests that the probable presence of sticker aggregates is not significantly reduced by the incorporation of NPs. In that case, one may have expected a drop of the plateau modulus (possibly detectable at 1 vol % in the NPs). These experiments therefore emphasize the competition existing between sticker association and adsorption onto NPs that could be investigated more in-depth with the help of model colloids characterized by a narrow size distribution and a well-controlled surface chemistry.

At lower frequency, the impact of NPs is much stronger and qualitatively similar to the previous case. In fact, the terminal relaxation is postponed to a much longer time (not visible in the probed window, including for 1 vol % in NPs), indicative of the formation of more stable TPy−Fe^{2+} bonds. TPy−Fe^{2+} complexes have indeed a much longer lifetime than TPy−Zn^{2+} ones.[9,13] A deeper rheological analysis consisting of probing lower frequencies and performing creep experiments for a whole day would certainly be of interest in a future work. In particular, the identification of a secondary plateau before the terminal regime would provide important information about the density and lifetime of TPy−NP bonds.

Beyond rheological characterization, the favorable interactions between the TPy functions and the NPs surface is further investigated through DSC, as presented in Figure 7 for both series of nanocomposites. Here, the raw signal is systematically normalized by the mass of the polymer in order to allow the emergence of possible variations of its C_p with increasing NP content. Similarly as in Figure 4A, C_p signals are fitted with a dose−response function and the corresponding ΔC_p^* values are represented in the insets of Figure 7A,B for PnBA−TPy(0.5)- and PnBA−TPy(2)-based nanocomposites, respectively. An increase in the NP content in PnBA−TPy(0.5) is seen to slightly decrease the ΔC_p^*, indicating that, in spite of much longer terminal relaxation time, the mobility of the chain segments is not dramatically affected by the presence of NPs. In other words, while the TPy−NP interactions appear to be much more stable than their TPy−Zn^{2+} counterparts, their number density must be quite low. The best evidence of this is that the data measured for PnBA−TPy(0.5)-5% can be successfully recalculated through a weighted average of the respective C_p of neat PnBA−TPy and Fe NP (dashed line in Figure 7A). Although a similar qualitative trend is observed in the case of PnBA−TPy(2)-based nanocomposites, ΔC_p^* exhibits a more pronounced diminution upon increasing the filler content, suggesting that chain segments suffer from a higher degree of steric hindrance. This quantitative difference is further supported by the fact that the weighted average C_p calculated from the neat components results in a higher ΔC_p^* than what is actually measured here (dashed line in Figure 7A).

3.3. Induction Heating of Nanocomposites. While we have used induction heating recently with the aim to stimulate the healing of thermoplastic elastomers for engineering applications,[34] we here combine it with thermal imaging to probe the properties of our supramolecular networks. In Figure 8, we report the evolution of the temperature as a function of time for three PnBA−TPy(0.5) nanocomposites loaded with 1, 3, and 5 vol % of Fe NPs. As one may have expected, an increase in the filler content leads to a larger heat production resulting in a higher maximum temperature. Since Fe NPs are ca. 90 nm in diameter, they are expected to contain several magnetic domains that will rearrange upon the application of the 855 kHz oscillatory magnetic field, being at the origin of

https://doi.org/10.1021/acs.macromol.2c00256
Macromolecules XXXX, XXX, XXX−XXX

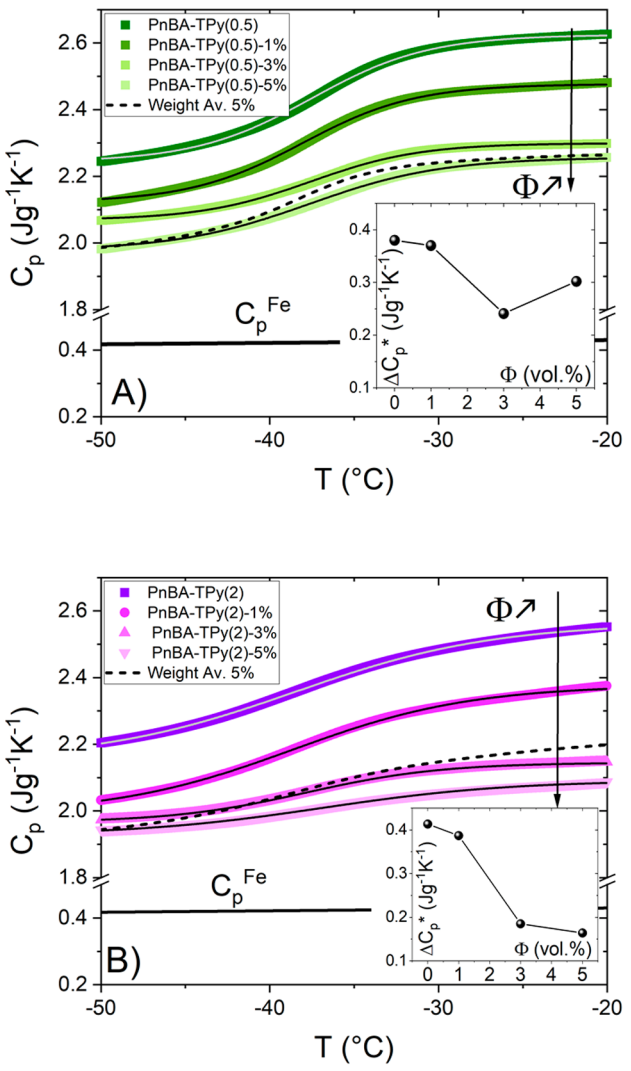

Figure 7. DSC thermograms of PnBA−TPy-based nanocomposites and their corresponding neat matrices, (A) PnBA−TPy(0.5) and (B) PnBA−TPy(2). The heat capacity is systematically normalized by the mass of the polymer within the composites. The theoretical signal of Fe NPs is also represented (C_p^{Fe}). Black thin solid lines are fitted to the data with the dose−response function providing the amplitude of the C_p step at the glass transition (ΔC_p^*) as represented in the inset as a function of the volume fraction of the particles. Dashed lines are calculated weight averages based on the signal of the neat matrix and C_p^{Fe}, assuming a filler content of 5 vol % (i.e., ≈30 wt %). These lines are vertically shifted onto the corresponding data at low temperature for clarity.

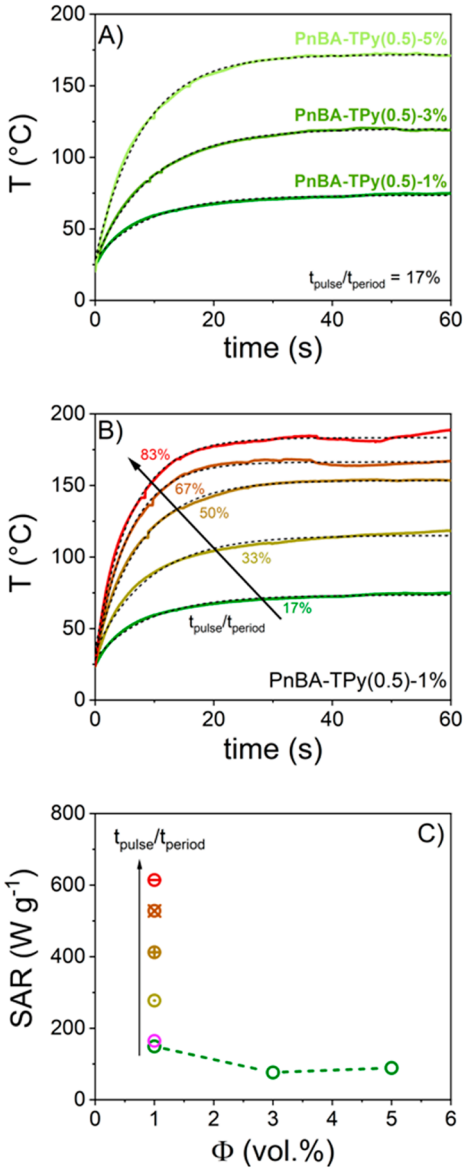

Figure 8. Thermal imaging during induction heating. (A) Impact of the filler fraction in a PnBA−TPy(0.5) matrix. (B) Impact of the pulsation time on PnBA−TPy(0.5)-1%. Dashed lines in (A) and (B) are fit to the data with eq 2. (C) Corresponding specific absorption rate (SAR). The purple ring indicates the value for PnBA−TPy(2)-1% at t_{pulse}/t_{period} = 17%.

the heat production (magnetic hysteresis losses). Remarkably, the $T(t)$ curves can be fitted successfully with a single exponential rise function

$$T(t) = T_0 + \Delta T(1 - e^{-t/\tau}) \quad (2)$$

where T_0 is the room temperature, ΔT is the amplitude of the temperature step, and τ is the characteristic time of the exponential rise. This expression, which is the 0-dimension solution of the heat equation for a constant energy flux, therefore indicates that the amount of heat generated by the time unit is constant during the experiment, possibly corresponding to a single heat source. Moreover, the focus on the PnBA−TPy(0.5)-1% formulation and an increase in the pulse duration of the magnetic field provides us with similar temperature trends, as shown in Figure 8B where the maximal temperature increases quasi-linearly with the pulse duration, t_{pulse} (the time between two consecutive pulses is denoted t_{period}). From all these temperature profiles, one can easily extract the specific absorption rate (SAR) corresponding to the power dissipated per gram of Fe powder as

$$SAR = \frac{C_p^{Fe}}{x_p} \frac{dT}{dt}\bigg|_{t\to 0} \quad (3)$$

where x_p is the mass fraction of Fe NPs in the nanocomposite.[47] The corresponding values are reported in Figure 8C where the SAR value is roughly constant when increasing the filler content, indicating limited dipolar interactions

https://doi.org/10.1021/acs.macromol.2c00256
Macromolecules XXXX, XXX, XXX−XXX

between the nanoparticles, as one may have anticipated from the reasonably low filler fraction. On the other hand, SAR values are expectedly growing linearly with the magnetic pulsation time, i.e., the time during which NPs are irradiated. These values, around 105 W g^{-1} on average for t_{pulse}/t_{period} = 17%, are in fair agreement with the ones reported in our previous work for similar particles (85 W g^{-1} on average)[34] embedded in a semicrystalline TPU; we assign the difference to the viscosity of the host matrix (see below).

Beyond the results presented in Figure 8, it is worth investigating the ability of the particles to heat samples upon dramatic changes of their environment (i.e., the matrix rheology), possibly providing us with additional information on the material's structure and interactions between the phases. In fact, while the heat production heavily depends on the intrinsic properties of the magnetic particles like their chemical nature and size, the viscosity of the surrounding medium is also expected to play a major role as it affects particle mobility.[48] While spontaneous rotation known as *Brownian relaxation* is excluded in our case because of the relatively high viscosity of the supramolecular networks, we evidenced that magnetic irradiation was able to stimulate spherical particle motion in thermoplastic elastomers, immediately following their melting point.[34] Because of the high frequency of the stimulus, this mechanism generates significant extra-heat through mechanical friction that is easily detectable through thermal imaging. For a given frequency of the magnetic field, the amplitude of this effect originates from the compromise between the rotation amplitude per time unit on one hand and the coefficient of friction with the surrounding medium on the other hand. While the former is promoted at low viscosity, the latter is more pronounced in highly viscous media, resulting in a possibly complex evolution of heat generation during the experiment, i.e., a complex $T(t)$ curve that cannot be rationalized through eq 2.

Following this logic, we present in Figure 9A the $T(t)$ curves measured from PnBA−TPy(0.5)-1% and PnBA−TPy(2)-1% for the same pulsation time. As mentioned above, the PnBA−TPy(0.5)-1% experiment leads to a simple exponential profile suggesting that the heat generated during the experiment is roughly constant. While magnetic domain motion is the dominating heat source, the SAR value we observe here (ca. 140 W g^{-1}) is significantly higher than in our previous study for the same conditions (ca. 82 W g^{-1} in arrested TPU). This significant difference indicates that the presence of mechanical friction (NP stimulated motion) from room temperature is highly plausible in the present case, being authorized by the not-so-viscous behavior of PnBA−TPy(0.5) (η_0(20 °C) ≈ 10^5 Pa s). Still, the absence of discontinuity in the profile indicates that no sudden drop in viscosity is happening. More interestingly, the same experiment performed on PnBA−TPy(2)-1% displays a quite different heating profile. First, the maximum temperature is strikingly higher than in PnBA−TPy(0.5)-1% while the NP content is almost identical (<8% relative difference). Second, the derivative of the $T(t)$ profile reported in Figure 9B unambiguously reveals a discontinuity in the temperature growth, reminiscent of a sudden change of viscosity felt by the particles. We believe here that these two effects are strongly correlated; we understand them as follows.

At the early stage (T < 50 °C), the temperature grows similarly in the two samples, mainly driven by the heat generated through magnetic hysteresis losses. During this period, PnBA−TPy(0.5)-1% heats slightly faster than PnBA−TPy(2)-1% likely due to its 10^4 times lower viscosity, allowing particles to partially rotate and produce heat through friction right from the beginning of the experiment. Then, from T = 50 °C, the temperature in PnBA−TPy(2)-1% becomes higher and dramatically increases to 80 °C (corresponding to ca. 15 s of induction heating). The failure of eq 2 to fit the data in Figure 9A (dashed line) and the corresponding derivative peak observed in Figure 9B are strong evidence of the apparition of a second heating mechanism in PnBA−TPy(2)-1%. We interpret this singularity as the sudden rotation of Fe particles, requiring a certain level of network dissociation. To support our interpretation, we provide in SI Section 2 additional examples of supramolecular networks showing similar $T(t)$ profiles during induction heating and briefly discuss their differences. To sum up, the key message is that while, in PnBA−TPy(0.5)-1%, the particle motion happens continuously from 20 °C due to the loose nature of the network, the particle rotation in the more densely cross-linked PnBA−TPy(2)-1% is triggered at higher temperatures, upon sufficient TPy−Zn^{2+} and TPy−NP bond dissociations.

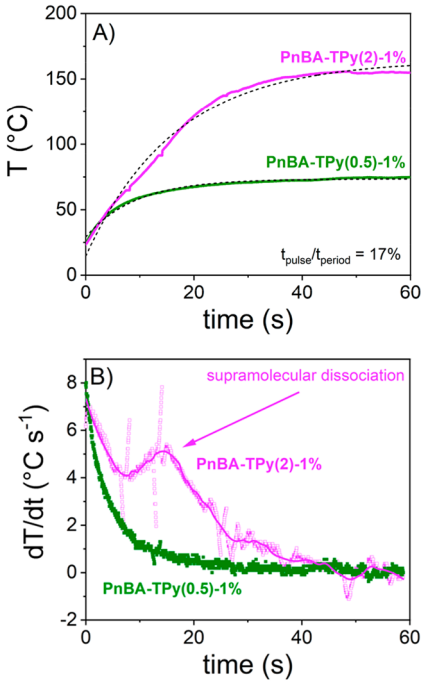

Figure 9. Thermal imaging during induction heating. (A) PnBA−TPy(0.5)-1% vs PnBA−TPy(2)-1%. Black dashed lines are fit to the data with eq 2. (B) Corresponding derivative signals.

This scenario is illustrated in Figure 10 where the cross-linking density of the network ($d_{network}$), including both TPy−Zn^{2+} and TPy−NP bonds, is expected to decrease exponentially with increasing temperature due to the Arrhenius dynamics of the supramolecular bonds. Importantly, the network density at low temperature is known to be much lower in PnBA−TPy(0.5)-1% than in PnBA−TPy(2)-1%, not only because of the amount of active TPy−Zn^{2+} bonds but also because of their aggregation of Zn^{2+} content, resulting in multifunctional cross-linking nodes. In addition, DSC suggested more favorable interactions between the matrix and NPs in PnBA−TPy(2)-1%, supporting an even greater supramolecular bond density in this sample. Besides, we hypothesize that the suddenness of the extra-heating mechanism observed in PnBA−TPy(2)-1% is related to the

https://doi.org/10.1021/acs.macromol.2c00256
Macromolecules XXXX, XXX, XXX−XXX

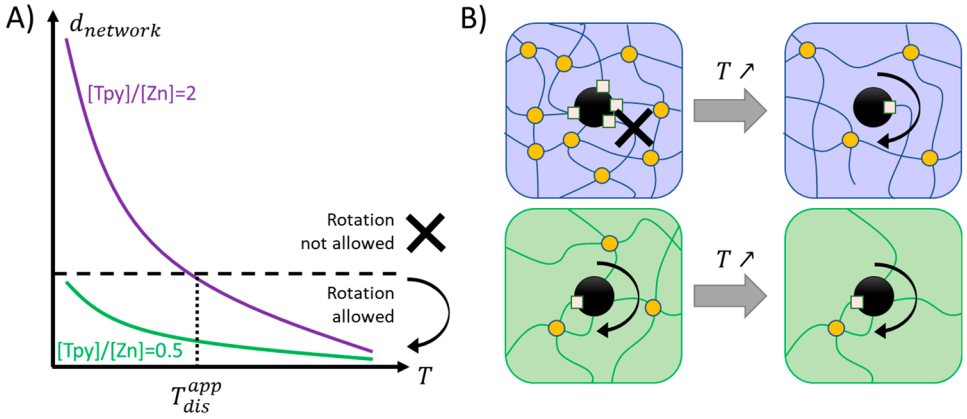

Figure 10. Scenario explaining the thermal imaging observations. (A) Cross-linking density of the network as a function of temperature for low- and high-density supramolecular matrixes. The black cross and arrow indicate, respectively, that rotation is blocked and allowed. (B) Schematic representation of the network surrounding an Fe particle. Orange disks and pinkish squares represent the TPy−Zn^{2+} complexes and the TPy adsorption site at the NP surface.

slope of $d_{network}$ at $T = T_{dis}^{app}$, the latter being the apparent dissociation temperature corresponding to the peak observed in Figure 9B. As illustrated in Figure 10A, an increase in the density of the network above a certain threshold should then result in a higher temperature of dissociation together with a sharper profile. The validity of this idea could be tested in the future through a systematic variation of the ratio [Zn]/[TPy] in composites loaded with a constant fraction of NP.

4. CONCLUSIONS

Linear rheology and calorimetry experiments have been performed on a series of supramolecular networks made of unentangled PnBA−TPy and Zn^{2+} ions with the aim to investigate their dynamics. While the sole PnBA−TPy behavior can be described using the usual WLF formalism, the formation of the supramolecular network results in an Arrhenius-like dynamics above the glass transition. Interestingly, while the value of T_g is not significantly impacted by the concentration in Zn^{2+} ions, i.e., by the density of the network, the corresponding jump of heat capacity ΔC_p^* dramatically drops, indicating strong dynamic heterogeneities reminiscent of other supramolecular systems. Besides, our thermomechanical characterization strongly suggests the aggregation of supramolecular moieties, supporting previous observations on metallo-supramolecular systems.

To complete the characterization of these materials and possibly open new ways for the design of smart nanocomposites, we then filled the PnBA−TPy networks with a low amount of Fe nanoparticles (Φ < 5 vol %). Strikingly, we revealed that, in addition to their strong interaction with Zn^{2+} ions, TPy moieties were able to interact favorably with NPs, probably through the formation of TPy−Fe^{2+} complexes, as suggested by the purple color of the as-prepared materials. In spite of a modest growth of the plateau modulus due to low filler content, the incorporation of TPy−NP interactions dramatically increases the terminal relaxation time and decreases ΔC_p^* compared to networks relying solely on TPy−Zn^{2+} interactions.

Last but not least, induction heating behavior, which offers opportunities in terms of materials engineering, notably concerning repeated healing of strong materials, was investigated using a thermal imaging technique. The analysis of the resulting $T(t)$ curves evidenced that the architecture of the network strongly impacts the heat production. It notably revealed a sudden increase of temperature around 80 °C in the densest network, which can be attributed to the massive dissociation of supramolecular bonds, permitting NP motions and heat production through mechanical friction. This original method, reminiscent of magneto-rheology with the difference that it is applicable to strong materials, offers new perspectives for the characterization of associated systems, completing more usual rheology and DSC experiments.

■ ASSOCIATED CONTENT

Supporting Information

The Supporting Information is available free of charge at https://pubs.acs.org/doi/10.1021/acs.macromol.2c00256.

Rheological data including all frequency sweeps used to build the master curves, a focus on the Rouse relaxation regime of the master curves showing the slight failure of the TTS caused by the thermorheological complexity of the networks, and an alternative master curve of the densest network (PnBA−TPy(2)) built from the a_T shift factors extracted from the neat PnBA−TPy matrix (highlighting the strong impact of the associative groups on the polymer dynamics over the whole temperature range); thermal imaging measurements performed during induction heating for a series of thermoplastic elastomer-based nanocomposites (supporting the scenario proposed to rationalize the extra heating observed in the dense PnBA−TPy(2) network) (PDF)

■ AUTHOR INFORMATION

Corresponding Authors

Charles-André Fustin − *Institute of Condensed Matter and Nanosciences (IMCN), Bio and Soft Matter Division (BSMA), Université Catholique de Louvain, B-1348 Louvain-la-Neuve, Belgium;* orcid.org/0000-0002-3021-5438; Email: charles-andre.fustin@uclouvain.be

Guilhem P. Baeza − *Univ Lyon, 69621 Villeurbanne, France;* orcid.org/0000-0002-5142-9670; Email: guilhem.baeza@insa-lyon.fr

Authors

Liuyin Jiang − *Univ Lyon, 69621 Villeurbanne, France; Univ Lyon, F-69621 Villeurbanne, France*

https://doi.org/10.1021/acs.macromol.2c00256
Macromolecules XXXX, XXX, XXX−XXX

Pablo Griffiths − *Univ Lyon, 69621 Villeurbanne, France*
Julie Balouet − *Univ Lyon, 69621 Villeurbanne, France; Univ Lyon, F-69621 Villeurbanne, France*
Titouan Faure − *Univ Lyon, 69621 Villeurbanne, France*
Rowanne Lyons − *Institute of Condensed Matter and Nanosciences (IMCN), Bio and Soft Matter Division (BSMA), Université Catholique de Louvain, B-1348 Louvain-la-Neuve, Belgium*

Complete contact information is available at: https://pubs.acs.org/10.1021/acs.macromol.2c00256

Author Contributions

[‖]L.J. and J.B. are both considered to be first authors.

Funding

G.P.B. acknowledges the financial support of IDEX-Lyon and INSA Lyon through the program ELAN-ERC as well as the Institut Carnot I@L for the funding assigned to the project POMMADE. This work was partially supported by funding from the H2020 Programme (MARIE SKŁODOWSKA-CURIE ACTIONS) of the European Commission's Innovative Training Networks (H2020-MSCA-ITN-2017) under DoDy-Net REA Grant Agreement No. 765811 and from UCLouvain through an FSR grant for R.L.

Notes

The authors declare no competing financial interest.

■ ACKNOWLEDGMENTS

All the authors thank Florent Dalmas (INSA-Lyon) and the staff at the *Centre Lyonnais de Microscopie* (CLyM) at INSA-Lyon for their help regarding the characterization of the materials. J.B., T.F., and G.P.B. thank the staff of the IMP laboratory (INSA-Lyon) for their help during the work at Mateis (relocation of students and access to experimental facilities).

■ REFERENCES

(1) Zhang, Z.; Chen, Q.; Colby, R. H. Dynamics of associative polymers. *Soft Matter* **2018**, *14*, 2961−2977.
(2) Bentz, K. C.; Cohen, S. M. Supramolecular metallopolymers: from linear materials to infinite networks. *Angew. Chem., Int. Ed.* **2018**, *57*, 14992−15001.
(3) Yang, L.; Tan, X.; Wang, Z.; Zhang, X. Supramolecular polymers: historical development, preparation, characterization, and functions. *Chem. Rev.* **2015**, *115*, 7196−7239.
(4) Voorhaar, L.; Hoogenboom, R. Supramolecular polymer networks: hydrogels and bulk materials. *Chem. Soc. Rev.* **2016**, *45*, 4013−4031.
(5) Seiffert, S.; Kumacheva, E.; Okay, O.; Anthamatten, M.; Chau, M.; Dankers, P. Y.; Greenland, B. W.; Hayes, W.; Li, P.; Liu, R., et al. *Supramolecular polymer networks and gels*; Springer, 2015.
(6) Khare, E.; Holten-Andersen, N.; Buehler, M. J. Transition-metal coordinate bonds for bioinspired macromolecules with tunable mechanical properties. *Nature Reviews Materials* **2021**, *6*, 421−436.
(7) Winter, A.; Schubert, U. S. Synthesis and characterization of metallo-supramolecular polymers. *Chem. Soc. Rev.* **2016**, *45*, 5311−5357.
(8) Ghiassinejad, S.; Mortensen, K.; Rostamitabar, M.; Malineni, J.; Fustin, C.-A.; Van Ruymbeke, E. Dynamics and Structure of Metallo-supramolecular Polymers Based on Short Telechelic Precursors. *Macromolecules* **2021**, *54*, 6400−6416.
(9) Brassinne, J.; Stevens, A. M.; Van Ruymbeke, E.; Gohy, J.-F.; Fustin, C.-A. Hydrogels with dual relaxation and two-step gel−sol transition from heterotelechelic polymers. *Macromolecules* **2013**, *46*, 9134−9143.
(10) Zhuge, F.; Brassinne, J.; Fustin, C.-A.; Van Ruymbeke, E.; Gohy, J.-F. Synthesis and rheology of bulk metallo-supramolecular polymers from telechelic entangled precursors. *Macromolecules* **2017**, *50*, 5165−5175.
(11) Falco, G.; Griffiths, P.; Coutouly, C.; Fustin, C.-A.; Baeza, G. P. Supramolecular Superparamagnetic Nanocomposites Based on a Magnetite-Filled Unentangled Terpyridine-Functionalized Polymer. *Macromolecules* **2020**, *53*, 5361−5370.
(12) Es Sayed, J.; Meyer, C.; Sanson, N.; Perrin, P. Oxidation-Responsive Emulsions Stabilized by Cleavable Metallo-Supramolecular Cross-Linked Microgels. *ACS Macro Lett.* **2020**, *9*, 1040−1045.
(13) Lewis, R. W.; Malic, N.; Saito, K.; Evans, R. A.; Cameron, N. R. Ultra-high molecular weight linear coordination polymers with terpyridine ligands. *Chemical science* **2019**, *10*, 6174−6183.
(14) Habicht, A.; Czarnecki, S.; Rossow, T.; Seiffert, S. Connectivity defects enhance chain dynamics in supramolecular polymer model-network gels. *J. Polym. Sci., Part B: Polym. Phys.* **2017**, *55*, 19−29.
(15) Bode, S.; Enke, M.; Bose, R.; Schacher, F.; Garcia, S.; Van Der Zwaag, S.; Hager, M.; Schubert, U. Correlation between scratch healing and rheological behavior for terpyridine complex based metallopolymers. *Journal of Materials Chemistry A* **2015**, *3*, 22145−22153.
(16) Louhichi, A.; Jacob, A.; Bouteiller, L.; Vlassopoulos, D. Humidity affects the viscoelastic properties of supramolecular living polymers. *J. Rheol.* **2017**, *61*, 1173−1182.
(17) Creton, C. 50th anniversary perspective: networks and gels: soft but dynamic and tough. *Macromolecules* **2017**, *50*, 8297−8316.
(18) Long, R.; Hui, C.-Y.; Gong, J. P.; Bouchbinder, E. The fracture of highly deformable soft materials: A tale of two length scales. *Annual Review of Condensed Matter Physics* **2021**, *12*, 71−94.
(19) Mayumi, K.; Marcellan, A.; Ducouret, G.; Creton, C.; Narita, T. Stress−strain relationship of highly stretchable dual cross-link gels: separability of strain and time effect. *ACS Macro Lett.* **2013**, *2*, 1065−1068.
(20) Yount, W. C.; Loveless, D. M.; Craig, S. L. Small-molecule dynamics and mechanisms underlying the macroscopic mechanical properties of coordinatively cross-linked polymer networks. *J. Am. Chem. Soc.* **2005**, *127*, 14488−14496.
(21) Zhao, J.; Mayumi, K.; Creton, C.; Narita, T. Rheological properties of tough hydrogels based on an associating polymer with permanent and transient crosslinks: Effects of crosslinking density. *J. Rheol.* **2017**, *61*, 1371−1383.
(22) Li, X.; Yang, Q.; Zhao, Y.; Long, S.; Zheng, J. Dual physically crosslinked double network hydrogels with high toughness and self-healing properties. *Soft Matter* **2017**, *13*, 911−920.
(23) Ahmadi, M.; Seiffert, S. Dynamic Model Metallo-Supramolecular Dual-Network Hydrogels with Independently Tunable Network Crosslinks. *J. Polym. Sci.* **2020**, *58*, 330−342.
(24) Gong, J. P. Why are double network hydrogels so tough? *Soft Matter* **2010**, *6*, 2583−2590.
(25) Chen, Q.; Chen, H.; Zhu, L.; Zheng, J. Engineering of tough double network hydrogels. *Macromol. Chem. Phys.* **2016**, *217*, 1022−1036.
(26) Nakajima, T. Generalization of the sacrificial bond principle for gel and elastomer toughening. *Polym. J.* **2017**, *49*, 477−485.
(27) Rose, S.; Dizeux, A.; Narita, T.; Hourdet, D.; Marcellan, A. Time dependence of dissipative and recovery processes in nanohybrid hydrogels. *Macromolecules* **2013**, *46*, 4095−4104.
(28) Rose, S.; Prevoteau, A.; Elzière, P.; Hourdet, D.; Marcellan, A.; Leibler, L. Nanoparticle solutions as adhesives for gels and biological tissues. *Nature* **2014**, *505*, 382−385.
(29) Fernández-de-Alba, C.; Jimenez, A. M.; Abbasi, M.; Kumar, S. K.; Saalwächter, K.; Baeza, G. P. On the Immobilized Polymer Fraction in Attractive Nanocomposites: T_g Gradient versus Interfacial Layer. *Macromolecules* **2021**, *54*, 10289−10299.
(30) Genix, A.-C.; Bocharova, V.; Kisliuk, A.; Carroll, B.; Zhao, S.; Oberdisse, J.; Sokolov, A. P. Enhancing the mechanical properties of glassy nanocomposites by tuning polymer molecular weight. *ACS Appl. Mater. Interfaces* **2018**, *10*, 33601−33610.

(31) Baeza, G. P.; Dessi, C.; Costanzo, S.; Zhao, D.; Gong, S.; Alegria, A.; Colby, R. H.; Rubinstein, M.; Vlassopoulos, D.; Kumar, S. K. Network dynamics in nanofilled polymers. *Nat. Commun.* **2016**, *7*, 11368.
(32) Chen, Q.; Gong, S.; Moll, J.; Zhao, D.; Kumar, S. K.; Colby, R. H. Mechanical reinforcement of polymer nanocomposites from percolation of a nanoparticle network. *ACS Macro Lett.* **2015**, *4*, 398−402.
(33) Cheng, S.; Sokolov, A. P. Correlation between the temperature evolution of the interfacial region and the growing dynamic cooperativity length scale. *J. Chem. Phys.* **2020**, *152*, No. 094904.
(34) Griffiths, P.; Coativy, G.; Dalmas, F.; Falco, G.; Jiang, L.; Xiang, Z.; Le, M.-Q.; Ducharne, B.; Le Roy, D.; Méchin, F.; Bernard, J.; Meille, S.; Baeza, G. P. Ultrafast Remote Healing of Magneto-Responsive Thermoplastic Elastomer-Based Nanocomposites. *Macromolecules* **2022**, *55*, 831−843.
(35) Laukkanen, O.-V. Small-diameter parallel plate rheometry: a simple technique for measuring rheological properties of glass-forming liquids in shear. *Rheol. Acta* **2017**, *56*, 661−671.
(36) Zhuge, F.; Hawke, L. G.; Fustin, C.-A.; Gohy, J.-F.; Van Ruymbeke, E. Decoding the linear viscoelastic properties of model telechelic metallo-supramolecular polymers. *J. Rheol.* **2017**, *61*, 1245−1262.
(37) Cui, G.; Boudara, V. A.; Huang, Q.; Baeza, G. P.; Wilson, A. J.; Hassager, O.; Read, D. J.; Mattsson, J. Linear shear and nonlinear extensional rheology of unentangled supramolecular side-chain polymers. *J. Rheol.* **2018**, *62*, 1155−1174.
(38) Chen, Q.; Tudryn, G. J.; Colby, R. H. Ionomer dynamics and the sticky Rouse model. *J. Rheol.* **2013**, *57*, 1441−1462.
(39) Leibler, L.; Rubinstein, M.; Colby, R. H. Dynamics of reversible networks. *Macromolecules* **1991**, *24*, 4701−4707.
(40) Jangizehi, A.; Ahmadi, M.; Seiffert, S. Emergence, evidence, and effect of junction clustering in supramolecular polymer materials. *Materials Advances* **2021**, *2*, 1425−1453.
(41) Mahmad Rasid, I.; Do, C.; Holten-Andersen, N.; Olsen, B. D. Effect of sticker clustering on the dynamics of associative networks. *Soft Matter* **2021**, *17*, 8960−8972.
(42) Neumann, L. N.; Gunkel, I.; Barron, A.; Oveisi, E.; Petzold, A.; Thurn-Albrecht, T.; Schrettl, S.; Weder, C. Structure−Property Relationships of Microphase-Separated Metallosupramolecular Polymers. *Macromolecules* **2020**, *53*, 5068−5084.
(43) Baeza, G. P. The reinforcement effect in well-defined segmented copolymers: Counting the topological constraints at the mesoscopic scale. *Macromolecules* **2018**, *51*, 1957−1966.
(44) Vilà, N.; Walcarius, A. Bis (terpyridine) Iron (II) Functionalized Vertically-Oriented Nanostructured Silica Films: Toward Electrochromic Materials. *Frontiers in chemistry* **2020**, *8*, 830.
(45) Einstein, A. Berichtigung zu meiner arbeit: Eine neue bestimmung der moleküldimensionen. *Annalen der Physik* **1911**, *339*, 591−592.
(46) Smallwood, H. M. Limiting law of the reinforcement of rubber. *Journal of applied physics* **1944**, *15*, 758−766.
(47) Abenojar, E. C.; Wickramasinghe, S.; Bas-Concepcion, J.; Samia, A. C. S. Structural effects on the magnetic hyperthermia properties of iron oxide nanoparticles. *Progress in Natural Science: Materials International* **2016**, *26*, 440−448.
(48) Deatsch, A. E.; Evans, B. A. Heating efficiency in magnetic nanoparticle hyperthermia. *J. Magn. Magn. Mater.* **2014**, *354*, 163−172.

https://doi.org/10.1021/acs.macromol.2c00256
Macromolecules XXXX, XXX, XXX−XXX